ChemComm

COMMUNICATION

View Article Online
View Journal | View Issue

Cite this: *Chem. Commun.*, 2020, **56**, 2893

Received 11th January 2020,
Accepted 21st January 2020

DOI: 10.1039/d0cc00249f

rsc.li/chemcomm

A novel RGO/N-RGO supercapacitor architecture for a wide voltage window, high energy density and long-life *via* voltage holding tests†

Rajneesh Kumar Mishra,[a] Gyu Jin Choi,[a] Youngku Sohn,[b] Seung Hee Lee*[c] and Jin Seog Gwag*[a]

Here, we demonstrated a unique symmetric supercapacitor (SSC) device architecture based on reduced graphene oxide (RGO) and nitrogen-doped RGO (N-RGO) electrodes. The RGO/N-RGO SSC shows a wide voltage window (2.2 V), high energy density (106.3 W h kg^{-1}), and ultra-high power density (15184.8 W kg^{-1}). The RGO/N-RGO SSC also delivers outstanding stability of 95.5% over 10 000 galvanostatic charging–discharging tests and 90.5% over 8 h of voltage holding tests. Additionally, this work explores a better understanding of leakage current and self-discharge mechanisms, which justifies the excellent state of health of the RGO/N-RGO SSC device.

Human civilization development is associated with the thriving nature and advancements of science and technologies.[1] Nowadays, rapid depletion of non-renewable fossil fuels (coal and oil) and climate change have become serious concerns for the livelihood of the next-generation.[2] Thus, zero-emission renewable energy (wind, hydro and solar) systems can play a substantial role to replace dependence from non-renewable fossil fuels.[2] However, this needs low cost, long-life, reliable, and efficient grid-level energy storage devices, which are essential for developing a green and clean economy.[3] In this energy dependent-world, supercapacitors are considered as emerging next-generation renewable energy storage systems for various applications such as household electronic appliances and portable smart electronic gadgets, *etc.*[3] Supercapacitors have magnified remarkable attention because of their high power density (>than 10 kW kg^{-1}), high efficiency, long cycle life (>10^5 cycles), fast charging–discharging process, cost-effectiveness and environmental friendly nature.[1–4] However, they suffer from low energy density, which needs unique modifications in electrode materials to improve electrochemical properties of supercapacitors.

Nowadays, carbon-based nanomaterials like carbon nanoanions,[5] carbon nanofibers,[5] carbon nanotubes,[6] reduced graphene oxide,[6] graphene,[7] and nitrogen (N) modified graphene[7] are considered excellent electroactive electrode nanomaterials to deliver outstanding electrochemical properties of electrochemical capacitors. Among these, reduced graphene oxide has shown tremendous interest because of its fantastic electrical, thermal, and optical properties with numerous applications.[8] Since the nitrogen (N) heteroatom can considerably modify the physical and chemical properties of RGO, because of (i) two lone pair electrons (high electrochemical activity), (ii) the N-atom is more electronegative than the carbon atom and (iii) high electron density of the nitrogen atom compared with a carbon atom, which can improve the conductivity of the host materials.[8] Recently, many reports have focused on modifications in carbon electrode materials for energy storage device applications.[5–8] However, there are still many issues, such as self-discharge mechanisms, stability *via* voltage holding tests, leakage current to be addressed to realize their commercial applications.

In this communication, we investigated the nitrogen (N) heteroatom modified reduced graphene oxide (N-RGO) and RGO in a two-electrode system of a symmetric supercapacitor (SSC) device. The RGO/N-RGO SSC shows excellent electrochemical properties such as high energy density, long-life *via* galvanostatic charging–discharging (GCD) and voltage holding tests, ohmic leakage of charge and diffusion-controlled processes and deficiency in current by the capacitor itself. As per literature reports, this unique architecture of RGO/N-RGO SSC has not been studied yet. RGO & N-RGO synthesis, characterization, electrode preparation, and RGO/N-RGO SSC design fabrication is discussed in the ESI.†

Fig. 1(a and c) and (b and d) exhibit the TEM (transmission electron microscopy) and HRTEM (high-resolution TEM) images of RGO and N-RGO, respectively. Fig. 1(b_1 and b_2) show enlarged portions of the TEM image with lattice spacing 0.36 nm corresponding to the (002) plane [Fig. 1(b_3 and b_4)] of RGO. Fig. 1(d_1 and d_2) show the magnified areas of a TEM image of the (002)

[a] *Department of Physics, Yeungnam University, Gyeongsan, Gyeongbuk, 38541, South Korea. E-mail: sweat3000@ynu.ac.kr*
[b] *Department of Chemistry, Chungnam National University, Daejeon, South Korea*
[c] *Applied Materials Institute for BIN Convergence, Department of BIN Convergence Technology and Department of Polymer-Nano Science and Technology, Chonbuk National University, Jeonju, Jeonbuk 561-756, South Korea. E-mail: lsh1@jbnu.ac.kr*

† Electronic supplementary information (ESI) available. See DOI: 10.1039/d0cc00249f

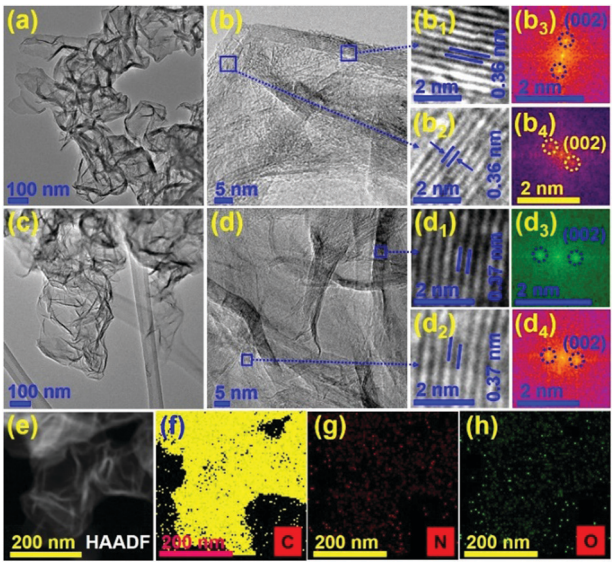

Fig. 1 (a) A TEM image and (b) a HRTEM image, with enlarged portions (b_1 and b_2) of the HRTEM image corresponding to FFT images (b_3 and b_4), of RGO. (c) A TEM image, (d) a HRTEM image, with enlarged portions (d_1 and d_2) of the HRTEM image corresponding to FFT images (d_3 and d_4), and (e) a HAADF image, with color mapping of (f) carbon (g) nitrogen, and (h) oxygen elements, of N-RGO.

plane with interplanar spacing 0.37 nm [Fig. 1(d_3 and d_4)] of N-RGO. Fig. 1(e and f–h) display the high-angle annular dark-field (HAADF) image and color mapping images of C, N and O elements of N-RGO. Also, Fig. S1 (ESI†) shows the color mapping of RGO corresponding respectively to nitrogen and oxygen elements. Fig. 2(a) describes the Raman vibrational phonon modes of RGO and N-RGO with two intense Raman bands of A_{1g} (D, 1352.2 cm^{-1}) and E_{2g} (G, 1583.1 cm^{-1}), respectively. The A_{1g} mode surfaces from the deformation of sp^2 hybridized carbon atom in RGO and N-RGO. However, the E_{2g} mode emerges due to the in-plane stretching of C–C vibrational phonon modes in RGO and N-RGO.[8] Fig. 2(b–d) show the XPS characteristic peaks of C1s (carbon), N1s (nitrogen), and O1s (oxygen) of N-RGO. Fig. 2(b) describes fitting of the carbon (C1s) peak consistent with C–C, C–N, and C–O of N-RGO. Fig. 2(c) explains the fitting of nitrogen (N1s) peak at 399.0 eV (pyridinic-N), 399.9 eV (pyrrolic-N), and 401.7 eV (graphitic-N) features of N-RGO. Fig. 2(d) shows the fitting of oxygen (O1s) peak with O–C═O (530.9 eV), C–OH (531.8 eV), and C═O (533.2 eV) is characteristics of N-RGO. Fig. S2 (ESI†) depicts the XPS spectra and the magnified portion of the N peak of RGO and N-RGO. Fig. S3 (ESI†) shows the fittings of characteristic peaks of carbon (C1s) and oxygen (O1s) of RGO.[9]

The electrochemical behavior of RGO and N-RGO electrodes in the three-electrode system is shown in Fig. S4–S6 (ESI†). Fig. 3(a) shows cyclic voltammetry (CV) curves of a RGO/N-RGO based symmetric supercapacitor (RGO/N-RGO SSC) with a wide potential window of 2.2 V. Fig. 3(b) depicts the cathodic and anodic CV peak fittings to discuss the capacitive storage and diffusion-limited process of charge storage kinetics [eqn (S1), ESI†] of RGO/N-RGO SSC. The *m*-values (slopes) are 0.54 and 0.75 at a scan rate range 10–50 mV s^{-1}, indicating a mixed

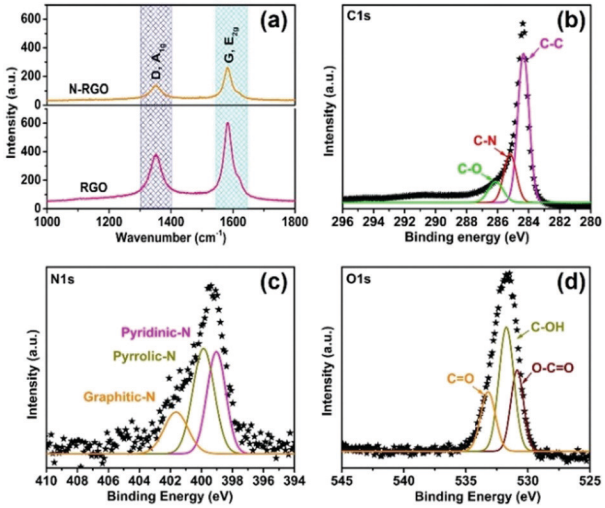

Fig. 2 (a) Raman spectra of RGO and N-RGO, and XPS narrow scan spectra of the (b) carbon C1s, (c) nitrogen N1s, and (d) oxygen O1s peaks of N-doped RGO.

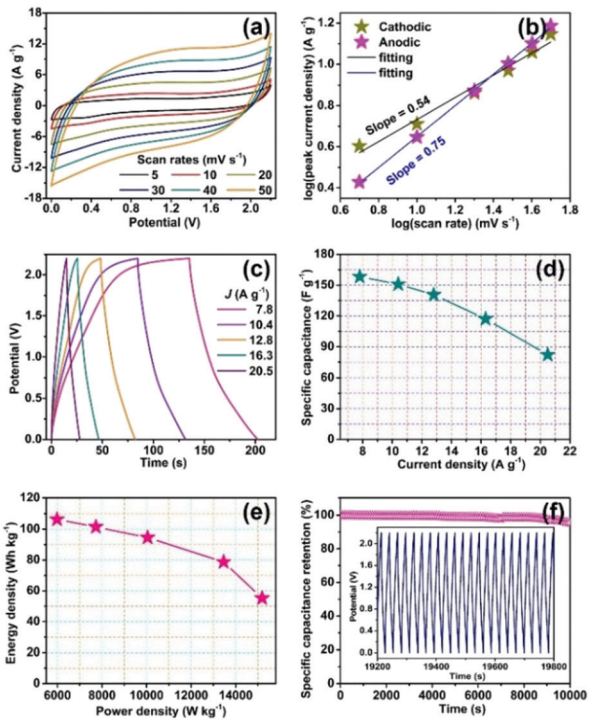

Fig. 3 RGO/N-RGO SSC: (a) CV curves, (b) log(current density) *vs.* log(scan rates) plots, (c) GCD plots, (d) specific capacitance and (e) energy density *vs.* power density plots, and (f) the stability over 10 000 GCD cycles at a current density of 20.5 A g^{-1}.

capacitive storage and diffusion-limited process of charge storage kinetics of RGO/N-RGO SSC. Therefore, the SSC device indicates a high rate capability due to the large scale contribution of capacitive nature over diffusion-limited processes.[9] Fig. 3(c) demonstrates the galvanostatic charging/discharging (GCD) plots of RGO/N-RGO SSC at distinct current density with a wide potential of 2.2 V. The GCD plots show the mixed

plateau-like and triangular shape, which features the existence of pseudocapacitance as well as EDLC (electrical double-layer capacitance), arising from electron transfer between the electrode material and electrolyte.[3,9] Further, the specific capacitance of RGO/N-RGO SSC was evaluated by using eqn (S2) (ESI†) and the area under the discharge GCD curve [Fig. 3(c)]. From Fig. 3(d), the calculated specific capacitance (current density) of RGO/N-RGO SSC is 158.2 (7.8), 150.9 (10.4), 140.6 (12.8), 117.1 (16.3) and 82.2 F g^{-1} (20.5 A g^{-1}). Fig. 3(e) portrays the energy density plot of RGO/N-RGO SSC, which was estimated by eqn (S3) and (S4) (ESI†). The RGO/N-RGO SSC transports high energy densities of 106.3, 101.4, 94.5, 78.7 and 55.2 W h kg^{-1} at power densities of 5981.0, 7725.2, 10045.7, 13456.2 and 15184.8 W kg^{-1}, respectively. These energy (powers) densities are competitive compared to recent reports, such as RGO 22.1 W h kg^{-1} (407.6 W kg^{-1}),[10] N-RGO 28.2 W h kg^{-1} (386.5 W kg^{-1}),[10] nitrogen-doped graphene sheets 80.5 W h kg^{-1} (558 W kg^{-1})[11] and graphene films 15.4 W h kg^{-1} (554 W kg^{-1}),[11] *etc.* Fig. 3(f) manifests good long-life (95.5%) of RGO/N-RGO SSC *via* 10 000 GCD cycles at 20.5 A g^{-1} (inset: in-between cycles).

This behavior is because of the following reasons: (i) high accessibility of the electrolyte-gel (PVA/Na_2SO_4) and negligible ion transfer resistance and (ii) enhanced surface wettability, interface compatibility between electrode/electrolyte and enhanced electrical conductivity due to N-atom doping.[12]

In addition to a GCD long-life test, Fig. 4(a) depicts the GCD cycling (4 cycles) + 2 h voltage holding tests (VHTs) and repeated tests for 8 h [inset: four GCD cycles after 6 h VHTs]. Fig. 4(b) shows the specific capacitance and its retention of RGO/N-RGO SSC at different VHTs times. The estimated values of the specific capacitance of RGO/N-RGO SSC are 82.3, 78.9, 78.0, 76.5, and 74.5 F g^{-1} at 2, 4, 6, and 8 h of VHTs, respectively. RGO/N-RGO SSC shows good specific capacitance retention (90.5%) after 8 h VHTs at 20.5 A g^{-1}. Moreover, Fig. 4(c) unveils the repeatability of three different RGO/N-RGO SSCs by VHTs. Inset in Fig. 4(c) portrays the GCD cycles (at 20.5 A g^{-1}) of three RGO/N-RGO SSCs after 4 h VHTs. GCD shows electrical double layer capacitance (EDLC) and pseudocapacitive (faradaic) characteristics that elucidate the overall capacitive nature of the RGO/N-RGO SSC. Fig. 2(c) shows the presence of pyridinic-N, pyrrolic-N/pyridone-N, and graphitic-N peaks in N-doped RGO, which can be responsible for pseudocapacitance in the RGO/N-RGO SSC.[13]

Moreover, leakage current and self-discharge are the important parameters to evaluate the practical importance of RGO/N-RGO SSC. In a constant voltage phase, the current through the stabilized

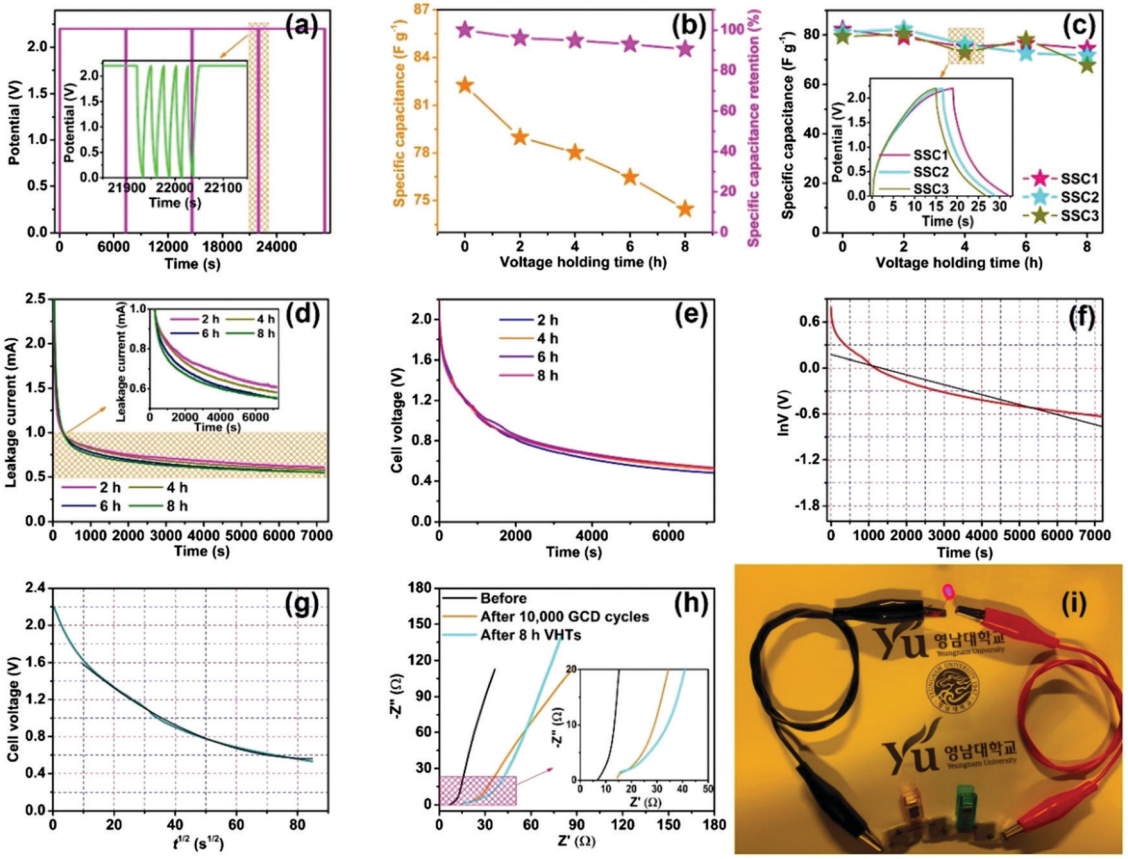

Fig. 4 The electrochemical performances of RGO/N-RGO SSC: (a) GCD cycling + voltage holding tests (VHTs) at 2.2 V, (b) specific capacitance and retention during VHTs, (c) reproducibility under VHTs, (d) leakage currents, (e) self-discharge, (f) self-discharge fitting (ohmic leakage of charge *via* a resistive pathway), (g) self-discharge fitting (diffusion-controlled process), (h) electrochemical impedance spectroscopy before/after 10 000 GCD cycles and 8 h of VHTs and (i) red LED illumination *via* connecting three SSCs in series.

RGO/N-RGO SSC compensates deficiency in the current by the capacitor itself, which can be called ''leakage current.'' Fig. 4(d) shows the leakage currents of RGO/N-RGO SSC recorded under voltage holding tests (VHTs) at different time ranges (inset depicts the enlarged portion of GCD cycles in between VHTs). The leakage current reduced significantly after a few seconds and then saturated. The values of leakage current evaluated under 2, 4, 6 and 8 h VHTs are 0.61 mA, 0.58 mA, 0.54 mA and 0.55 mA, respectively. The arise of leakage current in the RGO/N-RGO SSC may be due to the following reasons: (i) formation of impurities on both electrode surfaces during VHTs and (ii) surface oxygen-containing functional groups, *etc.*[14] The self-discharge mechanisms of RGO/N-RGO SSC mainly depended on two models: (i) ohmic leakage of charge *via* resistive pathways (potential driving model) [eqn (S5), ESI†] and (ii) diffusion-controlled variation of ion concentration [eqn (S6), ESI†].[14] Fig. 4(e) reveals the self-discharge curves (open-circuit voltage drop) for 2 h after being charged at 2.2 V for 2 minutes and repeated four times. Fig. 4(f) manifests the self-discharge curve (4th cycle, 8 h) and fitted by using eqn (S5) (ESI†) of RGO/N-RGO SSC. The self-discharge process is not regulated by the diffusion of charge carriers of RGO and N-RGO into the PVA/Na_2SO_4 electrolyte gel, but it decays exponentially *via* leakage of charge/redistribution *via* resistive pathways. The self-discharge plot is not well fitted with eqn (S5) (ESI†) of the potential driving model. Therefore, this self-discharge process of RGO/N-RGO SSC is not due to ohmic leakage of charge *via* resistive pathways. However, Fig. 4(g) signals the logarithm of the self-discharge voltage plot *vs.* the square root of time (4th cycle, 8 h), which fitted well with the diffusion-controlled process (eqn (S6), ESI†). In this process, after charging RGO/N-RGO SSC at 2.2 V for 2 minutes and then after that, the accumulated charges at the surface of RGO and N-RGO experience a redistribution process as well as diffusion of double-layer electrolyte ions from the RGO and N-RGO surface into the electrolyte. Therefore, the self-discharge results of RGO/N-RGO SSC elucidate the dominance of diffusion related reactions between electrolyte ions/electrode materials over leakage of charge.

Fig. 4(h) shows the electrochemical impedance spectroscopy (EIS) spectra of RGO/N-RGO SSC to unearth ion transport behavior as discussed in the ESI†. Also, Randles plots [Fig. S8, ESI†], and Bode plots [Fig. S9, ESI†] are studied and discussed in ESI† to justify the self-discharge mechanisms. Additionally, Table S1 (ESI†) indicates the comparative study of our RGO/N-RGO SSC with other reported RGO, graphene, and N-doped RGO SSC. Table S1 (ESI†) concludes that this work shows high energy density (106.3 W h kg^{-1}) with additional study of stability *via* VHTs and self-discharge process as compared with other reported works in the literature. Fig. 4(i) reveals the practical applicability of SSC by illuminating a red LED *via* connecting three RGO/N-RGO SSCs in series.

In conclusion, we assembled an RGO/N-RGO SSC, with RGO as one electrode and N-RGO as the second electrode; this was examined for its electrochemical properties, showing magnificent long-life properties following VHTs, and the self-discharge mechanisms were further explored. Thus, nitrogen doping might smartly tune the local electronic structures of RGO and, therefore, improve the energy density of the RGO/N-RGO SSC. Therefore, the RGO/N-RGO SSC is a potential energy storage medium for futuristic portable electronic gadgets.

This work was financially supported through the Basic Science Research Program by the National Research Foundation of Korea (NRF) funded by the Ministry of Science, ICT, and Future Planning (Grant No. 2019R1D1A3A03103662).

Conflicts of interest

There are no conflicts to declare.

Notes and references

1 (*a*) F. Wang, X. Wu, X. Yuan, Z. Liu, Y. Zhang, L. Fu, Y. Zhu, Q. Zhou, Y. Wu and W. Huang, *Chem. Soc. Rev.*, 2017, **46**, 6816–6854; (*b*) M. M. P. Madrigal, M. G. Edo and C. Alemán, *Green Chem.*, 2016, **18**, 5930–5956.
2 (*a*) T. Chen and L. Dai, *J. Mater. Chem. A*, 2014, **2**, 10756–10775; (*b*) G. Zhang, X. Xiao, B. Li, P. Gu, H. Xue and H. Pang, *J. Mater. Chem. A*, 2017, **5**, 8155–8186.
3 (*a*) Y. Zhang, J. He, Z. Gao and X. Li, *Nano Energy*, 2019, **65**, 104045; (*b*) R. K. Mishra, J. H. Ryu, H.-I. Kwon and S. H. Jin, *J. Mater. Chem. A*, 2018, **6**, 15253–15264; (*c*) M. Minakshi, M. J. Barmi and R. T. Jones, *Dalton Trans.*, 2017, **46**, 3588–3600.
4 (*a*) L. Liu, Z. Niu and J. Chen, *Chem. Soc. Rev.*, 2016, **45**, 4340–4363; (*b*) P. Simon and Y. Gogotsi, *Nat. Mater.*, 2008, **7**, 845.
5 (*a*) D. Mohapatra, G. Dhakal, M. S. Sayed, B. Subramanya, J.-J. Shim and S. Parida, *ACS Appl. Mater. Interfaces*, 2019, **11**, 8040–8050; (*b*) L.-F. Chen, X.-D. Zhang, H.-W. Liang, M. Kong, Q.-F. Guan, P. Chen, Z.-Y. Wu and S.-H. Yu, *ACS Nano*, 2012, **6**, 7092–7102.
6 (*a*) M. Kaempgen, C. K. Chan, J. Ma, Y. Cui and G. Gruner, *Nano Lett.*, 2009, **9**, 1872–1876; (*b*) J. R. Rani, R. Thangavel, S.-I. Oh, J. M. Woo, N. C. Das, S.-Y. Kim, Y.-S. Lee and J.-H. Jang, *ACS Appl. Mater. Interfaces*, 2017, **9**, 22398–22407.
7 (*a*) P. Xiong, J. Zhu, L. Zhang and X. Wang, *Nanoscale Horiz.*, 2016, **1**, 340–374; (*b*) Z. Wen, X. Wang, S. Mao, Z. Bo, H. Kim, S. Cui, G. Lu, X. Feng and J. Chen, *Adv. Mater.*, 2012, **24**, 5610–5616.
8 (*a*) J. Wu, Z. Pan, Y. Zhang, B. Wang and H. Peng, *J. Mater. Chem. A*, 2018, **6**, 12932–12944; (*b*) B. Lee, C. Lee, T. Liu, K. Eom, Z. Chen, S. Noda, T. F. Fuller, H. D. Jang and S. W. Lee, *Nanoscale*, 2016, **8**, 12330–12338.
9 (*a*) R. Ramkumar and M. M. Sundaram, *New J. Chem.*, 2016, **40**, 7456–7464; (*b*) P. Sun, W. He, H. Yang, R. Cao, J. Yin, C. Wang and X. Xu, *Nanoscale*, 2018, **10**, 19004–19013.
10 (*a*) R. K. Mishra, G. J. Choi, Y. Sohn, S. H. Lee and J. S. Gwag, *Mater. Lett.*, 2019, **253**, 250–254; (*b*) R. K. Mishra, G. J. Choi, Y. Sohn, S. H. Lee and J. S. Gwag, *Mater. Lett.*, 2019, **245**, 192–195.
11 (*a*) Y. Qiu, X. Zhang and S. Yang, *Phys. Chem. Chem. Phys.*, 2011, **13**, 12554–12558; (*b*) A. Yu, I. Roes, A. Davies and Z. Chen, *Appl. Phys. Lett.*, 2010, **96**, 253105.
12 (*a*) M. Wang, J. Yang, S. Liu, M. Li, C. Hu and J. Qiu, *J. Colloid Interface Sci.*, 2020, **560**, 69–76; (*b*) J. Han, Q. Li, C. Peng, N. Shu, F. Pan, J. Wang and Y. Zhu, *Appl. Surf. Sci.*, 2020, **502**, 144191.
13 Y.-H. Lee, K.-H. Chang and C.-C. Hu, *J. Power Sources*, 2013, **227**, 300–308.
14 (*a*) Q. D. Nguyen, Y.-H. Wu, T.-Y. Wu, M.-J. Deng, C.-H. Yang and J.-K. Chang, *Electrochim. Acta*, 2016, **222**, 1153–1159; (*b*) Z. Wang, X. Chu, Z. Xu, H. Su, C. Yan, F. Liu, B. Gu, H. Huang, D. Xiong, H. Zhang, W. Deng, H. Zhang and W. Yang, *J. Mater. Chem. A*, 2019, **7**, 8633–8640.

